A Novel Control System for Solar Tile Micro-Inverters

Nicholas Falconar, Dawood Shekari Beyragh, and Majid Pahlevani
Schulich School of Engineering
University of Calgary
Calgary, Alberta, Canada
Email: nwfalcon@ucalgary.ca

***Abstract*—This paper presents a sensorless peak current mode (PCM) control technique for a flyback photovoltaic (PV) micro-inverter. The micro-inverter is used to extract energy from rooftop solar tiles and deliver it to the utility grid. Current sensors are usually required in the micro-inverter circuitry in order to perform maximum power point tracking (MPPT), as well as in the current loop to shape the output current to a sinusoidal waveform synchronous with the utility grid. The proposed method in this paper is able to estimate the current mathematically, thus, eliminating the need for current sensors on the converter. This provides a practical and cost-effective solution for solar tile applications. Simulation and experimental results show the feasibility of the proposed technique and demonstrate its superior performance.**

I. Introduction

Solar energy offers a very clean and practical power generation method to the end-user [1]. Although PV panels have been the main devices to harvest solar energy, they have some disadvantages that may divert the market to other solutions for residential electricity demand. PV panels require high installation costs and they are not visually pleasing. These issues have inspired companies to integrate solar cells into construction components such as roof tiles. This integration is referred to as building integrated photovoltaics (BIPV), a design strategy that lowers the upfront cost of PV installations. Money saved by employing BIPVs is equivalent to the cost of the substituted building materials. Within the range of BIPVs available, PV tiles or PV shingles, used on solar roofs, have gained a lot of attention to fulfill residential energy demand. This is evidenced by the new solar tiles currently produced by Tesla [2].

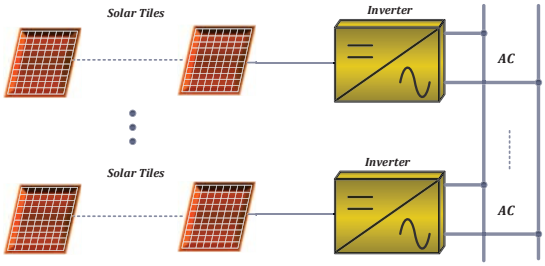

Fig. 1: Solar Tile PV Topologies

Solar inverters are power electronic converters that extract power from solar tiles and inject power to the utility grid.

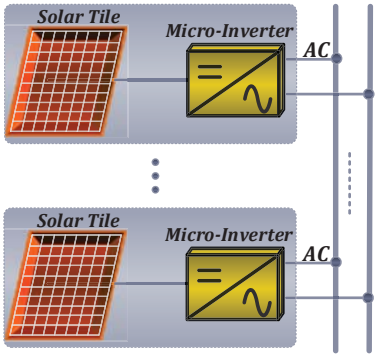

Fig. 2: Solar Tile PV Topologies

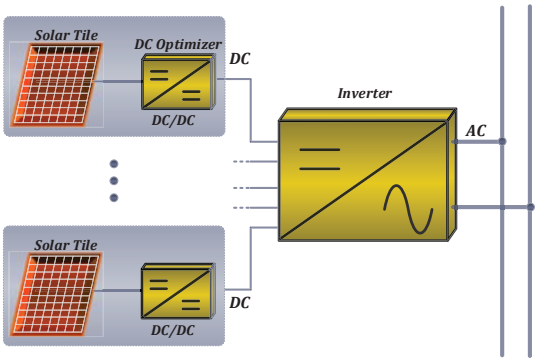

Fig. 3: Solar Tile PV Topologies

There are a few common approaches to implement solar inverters: string inverters, DC optimizers, and micro-inverters. Basic implementations of these topologies are seen in Figs. 1, 2, and 3. Advantages and disadvantages exist for each topology and the dominant option is not yet clear. String inverters suffer from partial shading, an obstacle that can drastically reduce the output power of a series-connected solar array. Partial shading is a phenomena experienced by series-connected solar modules where individual modules are forced away from their maximum power point (MPP) due to part of the array being shaded [3], [4]. Shade producing objects are often present above homes (e.g. trees, chimneys, other homes). Thus, string inverters are not an appropriate option for this application. DC optimizers seem to be a good option as they are able to avoid the partial shading obstable using module-level optimization

978-1-5386-1180-7/18/$31.00 ©2018 IEEE

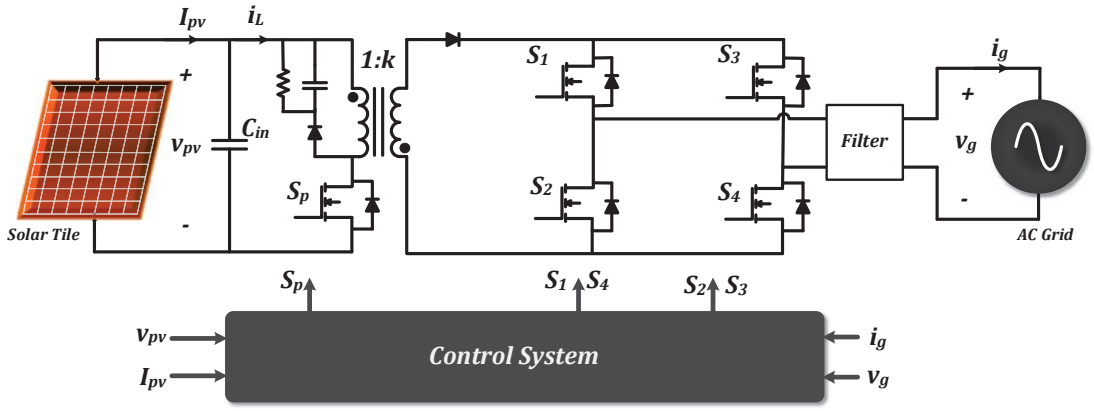

Fig. 4: Solar tile micro-inverter.

[5]. However, a problem arises in implementation: since this topology relies on a central inverter, a particular number of modules must be connected in order to maintain a correct input voltage to the inverter. Thus, there would need to be a specific layout plan designed for each house dependent upon the roof shape and size. Thus, it is not a plug-and-play option, with low flexibility and added design cost. PV micro-inverters seem to be the best option for this application since they individually optimize each tile and can all be in parallel at the output. The issue with PV micro-inverters is their high cost compared to other solutions. In this paper, a low-cost micro-inverter is proposed for solar tiles. The micro-inverter employs a new control system, which is able to eliminate current sensors from the micro-inverter circuitry. Usually, two current sensors are required for a PV micro-inverter: one measures the PV current for MPPT and the other senses the output current in order to shape it to a sinusoidal waveform synchronous with the grid voltage. These sensors are costly and introduce both noise and delay into the control system. The proposed method in this paper removes the need for current sensors, providing a practical and cost-effective solution for this application.

II. Solar Tile Micro-Inverter Functionalities

Since the cost is of great importance in solar tile applications, the micro-inverter power circuitry is based on the flyback converter topology [6]–[10]. Flyback converters are similar to buck-boost converters but employ a two-winding inductor. The flyback converter offers better isolation and higher voltage ratio capability. Fig. 4 shows the PV micro-inverter used for this application. The circuit includes a high frequency flyback circuit and a low frequency unfolding circuit. The control system operates both the high frequency flyback switch and the low frequency switches at the output. Output current grid-synchronization is performed by measuring output voltage at the frequency of the switching cycle and performing the necessary modifications to the unfolding circuit and duty cycle. MPPT is performed using the perturb and observe (P&O) method.

According to Fig. 4, the mathematical model of the system is given by:

$$\Sigma^{\mu Inv}: \begin{cases} \dfrac{di_L}{dt} = \dfrac{1}{L} v_{pv} S^p(t) \\ \dfrac{dv_{pv}}{dt} = \dfrac{1}{C_{in}} I_{pv} - \dfrac{1}{C_{in}} i_L S^p(t) \end{cases} \quad (1)$$

Where L is the inductance of the flyback transformer, and $S^p(t)$ is the switching function defined by:

$$S^p(t) = \begin{cases} 1 & when\ S_p\ is\ ON \\ 0 & when\ S_p\ is\ OFF \end{cases}$$

It should be noted that (1) is not an averaged model and it describes instantaneous chracteristics of the system. Eq. (1) describes a second order system (i.e., $\dot{X} = F(X,u)$ where $X = [x_1 = i_L, x_2 = v_{pv}]^T$, $u(t) = S^p(t)$, and $F = [x_2 u/L, I_{pv}/C_{in} - x_1 u/C_{in}]^T$). The objective is to design a current observer for i_L. Current observers can be used to optimize circuit design and improve performance in power electronics [11], [12]. In order to design the observer, the observability of the system should first be investigated. The observability of the system with respect to i_L is determined through the observability co-distribution defined by [13]–[17]:

$$\mathbf{dim}(d\mathcal{O}_{\mu Inv}) = \mathbf{dim} \begin{pmatrix} \nabla \mathcal{L}_F^0 h \\ \nabla \mathcal{L}_F^1 h \end{pmatrix} = \mathbf{rank} \begin{pmatrix} 0 & 1 \\ S^p(t)/C_{in} & 0 \end{pmatrix} \quad (2)$$

where the measurable state is $h = x_2 = v_{pv}$. According to (2), the dimension of the observability co-distribution is $\mathbf{dim}(d\mathcal{O}_{\mu Inv}) = 2$ everywhere except when $S^p(t) = 0$. When $S^p(t) = 0$, the rank collapses to 1 rendering i_L unobservable. Thus, the system is observable everywhere except when the flyback switch is OFF (corresponding to the zero crossings of the grid voltage as well as off time during each switching cycle). However, while $S^p(t) = 0$, the flyback switch becomes an open circuit and the only current through the inductor is a very small snubber current. Therefore: $i_L \approx 0$, when $S^p(t) = 0$ and requires no estimation.

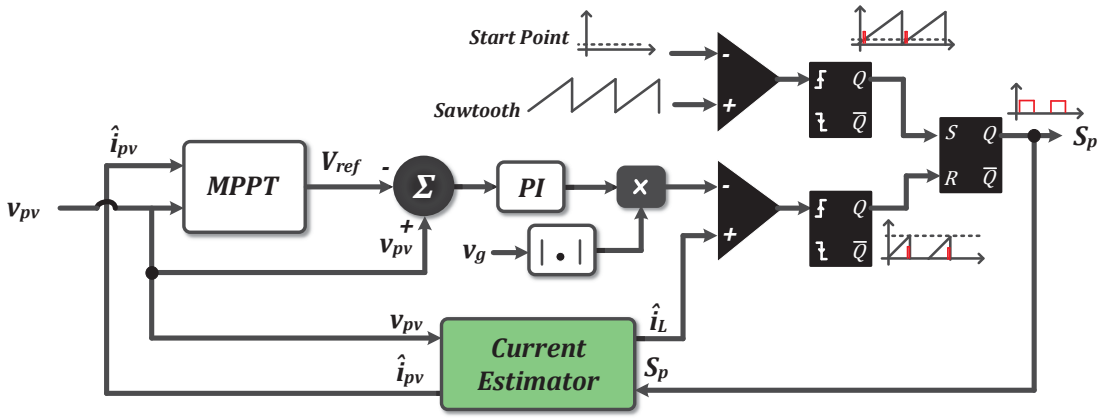

Fig. 5: Block diagram of the control system.

III. Proposed sensorless Peak Current Mode (PCM) Control Technique

In this section, a new control system is presented for the PV micro-inverter, implementing PCM control without using current sensors. A block diagram of the control system is illustrated in Fig. 5. According to Fig. 5, PCM is implemented only using measurements of PV voltage and grid voltage. The gate pulses are initiated by the top compator outputting clock pulses at the desired frequency for PWM. The gate pulses fall once estimated current has reached the desired magnitude. This magnitude is determined by the proportional integral (PI) controller output and the instantaneous rectified grid voltage (the peak current follows the shape of the rectified grid voltage). Additionally, a maximum T_{on} can be maintained by ORing the output of the bottom comparator with maximum T_{on}. Exceeding the circuit maximum T_{on} will push flyback operation into continuous conduction mode (CCM) causing instability in the system. The current estimator block estimates the instantaneous inductor current value using inputs of PV voltage and duty cycle. Calculation of PV current is also perfomed for input to the MPPT block. This calculation is done simply by taking a running average of the inductor current. The MPPT block uses the P&O method to determing a reference voltage from input PV voltage and estimated PV current, a PI controller is used to drive PV voltage to the desired reference voltage.

Fig. 6. shows the proposed current estimator. According to Fig.3, the current estimator calculates the current i_L based on the PV voltage and switching cycle. The current estimator is based on the precise model of the system given by (1). The update law for the proposed current observer is given by:

$$\hat{\Sigma}^{\mu Inv}: \begin{cases} \dot{\hat{i}}_L = \hat{\theta} v_{pv} S^p(t) \\ \dot{\hat{v}}_{pv} = \dfrac{1}{C_{in}} I_{pv} - \dfrac{1}{C_{in}} \hat{i}_L S^p(t) \\ \dot{\hat{\theta}} = \gamma v_{pv} \tilde{v}_{pv} \end{cases} \tag{3}$$

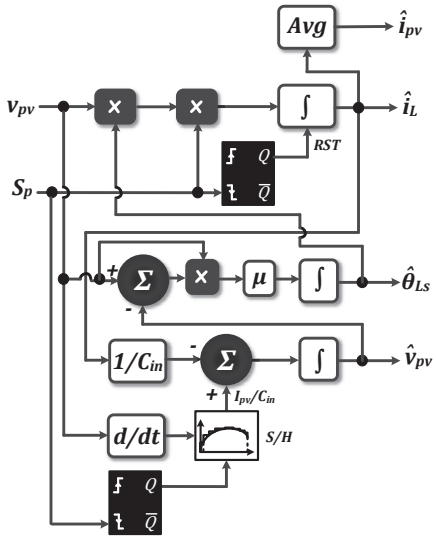

Fig. 6: Block diagram of the proposed current estimator.

where $\tilde{v}_{pv} = v_{pv} - \hat{v}_{pv}$. One of the prominent aspects of the proposed observer is its capability to track the value of the inductance L. The inductance value can vary significantly based on the operating conditions (e.g., temperature, frequency, etc.) as well as physical manufacturing differences limited by tolerance. Thus, in order to have an accurate estimation of the high frequency current, the value of the inductance should constantly be updated. The inductance value L is estimated based on the error of the PV voltage. The update law for the inductance value $\hat{\theta}$ is given in (3) where $\theta = 1/L$. The proposed observer also tracks the PV current by measuring the PV voltage. The PV voltage dynamics are given in (1)

According to (1), the change in PV voltage when the gate pulses are OFF (i.e., There is no current at the primary side, $i_L = 0$) is equal to I_{pv}/C_{in}. Thus, the estimation of the PV voltage, $\hat{v}_{pv}$, is based on the sample once the switch has turned

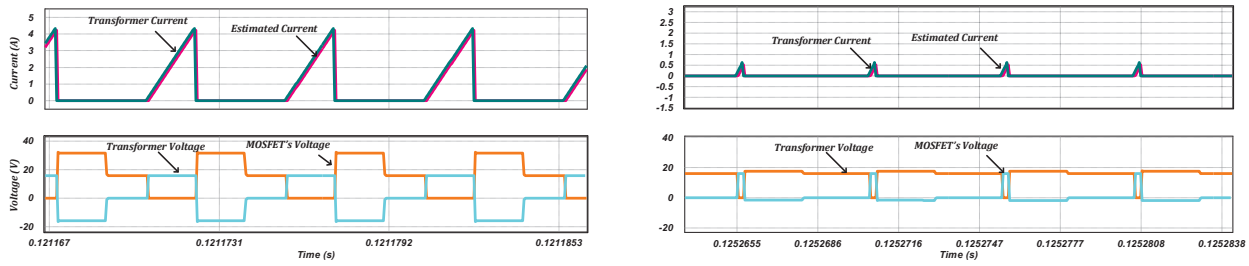

Fig. 7: Simulation results.

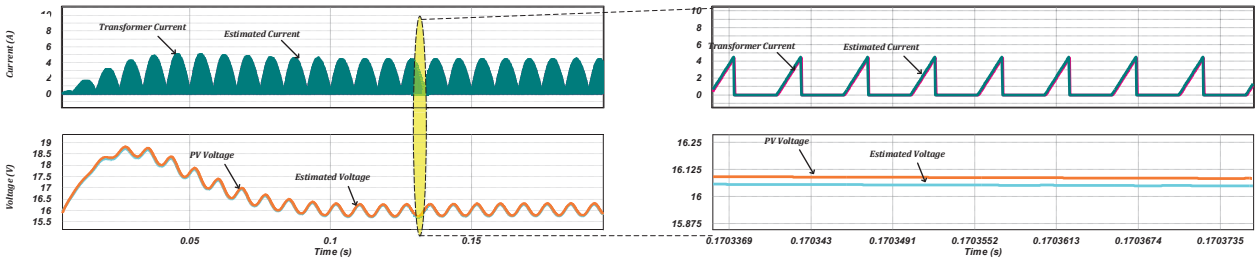

Fig. 8: Simulation results.

OFF (with some delay) and the estimated current $\hat{i}_L$. The PV current is the averaged value of i_L. Therefore, a digital filter (e.g., FIR) is used to estimate the PV current for the MPPT block.

IV. Simulation Results

In this section, simulation results of the proposed sensorless PCM controller are presented. The simulation was conducted on PSIM using the control block diagram depicted in Fig. 5 and the current estimator depicted in Fig. 6. A flyback micro-inverter circuit was constructed in the software, parameters for the circuit appear in TABLE I. Fig. 7 and 8 illustrate the simulation results of the online operation of the solar tile, micro-inverter, and control system. Fig. 7(a) and (b) demonstrate the high frequency waveforms of the inverter and the estimated current close to the peak of the AC line and near the zero crossing respectively. It is evident in Fig. 7 that the current estimator functions properly in the system. MPPT performance can be infered by convergence time of Fig. 8. In this test, MPPT converged in just over 0.1s, assuring good dynamic tracking efficiency. Fig. 8 also demonstrates PV voltage estimation. This figure illustrates that the tracking error is very low and MPPT is performed for the solar tile. According to the simulations, the system is able to track grid voltage by maintaining correct inductor current estimation throughout the line cycle.

V. Experimental Results

In this section, experimental results gathered from a solar tile micro-inverter operating with the proposed control system are analyzed. In order to verify the performance of the proposed inverter, an $8.7W$ experimental prototype of the solar tile micro-inverter has been implemented. The test was performed using a PV simulator (ETS80X10.5C manufactured by Ametek). Specifications for the micro-inverter appear in TABLE I. Specifications for the implemented solar module appear in TABLE II. The control system was implemented using an FPGA. Specifically, the Altera Cyclone IV was used, an FPGA that provides a fast and low-cost method to control power converters [18].

TABLE I: Specifications of Flyback Converter

Symbol	Parameter	Value
L	Inducatance	$6.4uH$
n	Turns ratio	16:340
C_{in}	Input Capacitance	$2000uF$
f_{sw}	Switching frequency	$200kHz$

TABLE II: Specifications of Module

Symbol	Parameter	Value
P_{max}	Maximum Power	$8W$
V_{oc}	Open Circuit Voltage	$20.12V$
V_{mp}	Voltage at MPP	$16.91V$
I_{sc}	Short Circuit Current	$0.55A$
I_{mp}	Current at MPP	$0.514A$

Measurements taken from the experimental circuit appear in Fig. 9. Fig. 9 (a) and (b) depict flyback switch operation at the edges of the duty cycle range. Experimental switch control and operation validate the simulation results confirming proper circuit and control system operation. In Fig. 9 (c) and (d), overall circuit operation and grid interaction are demonstrated. Both show output current synchronously tracking grid voltage

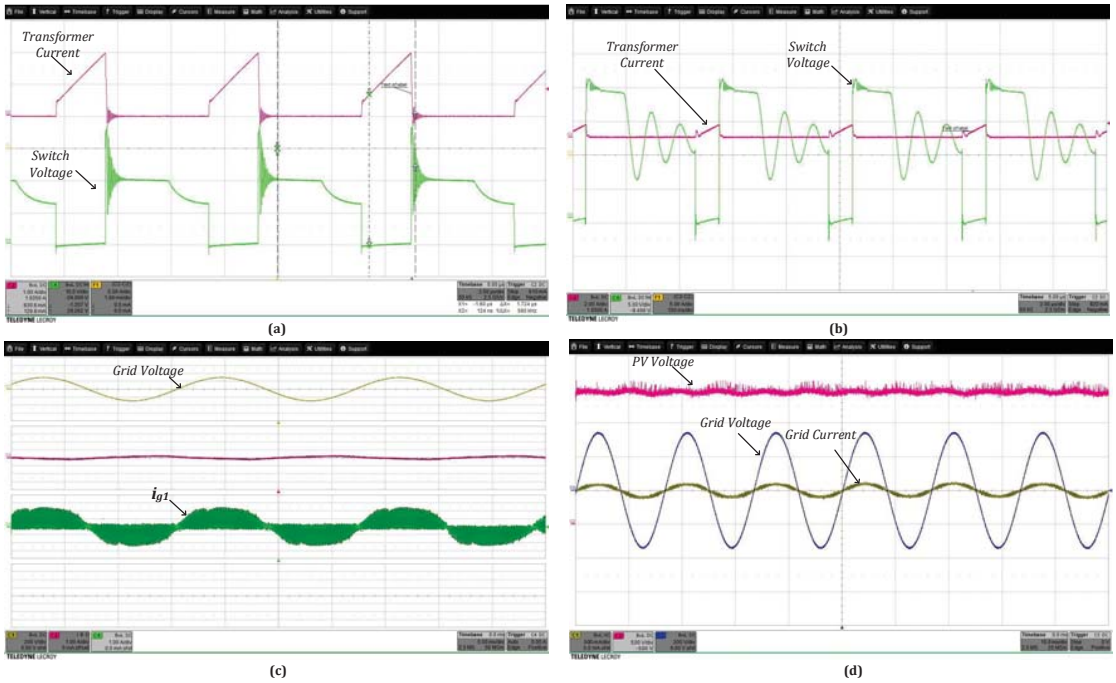

Fig. 9: Experimental results.

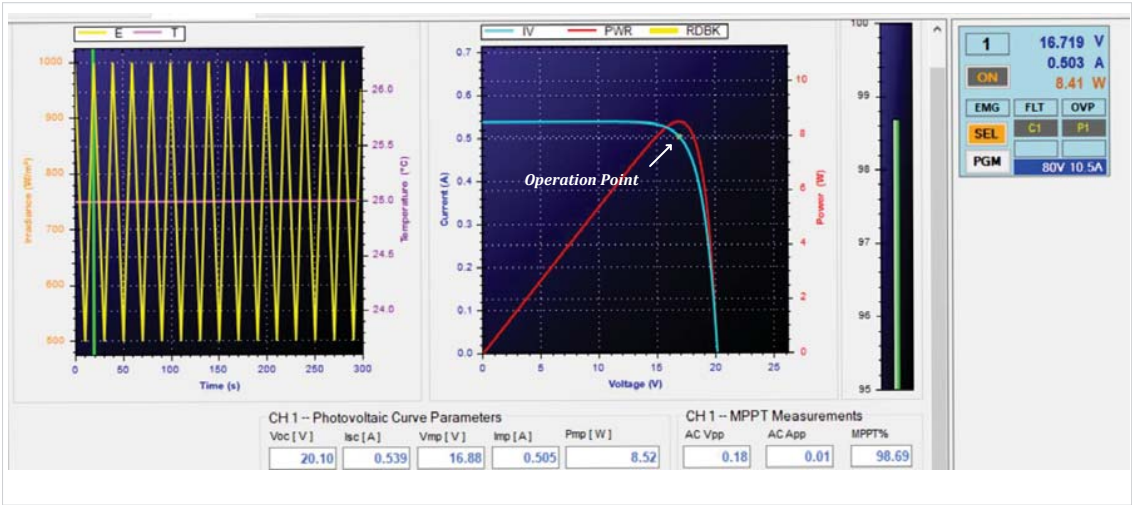

Fig. 10: Experimental results.

throughout the grid cycle, confirming correct operation of the control system. PV voltage appears in Fig. 9 (d), along with the PV voltage estimate, a double grid frequency ripple is present in the PV voltage. A screenshot of the software used for the PV simulation test is shown in Fig. 10. As seen in the figure, correct MPPT operation is attained. The test tracked MPPT performance while the module was subject to quickly varying irradiance, faster than natural changes. MPPT retained high dynamic tracking efficiencies througout the operation range of the micro-inverter. The performance of the control system in conjunction with MPPT is confimed to be both reliable and highly efficient.

According to the experimental results, the proposed control system can effectively control the micro-inverter without the need for current sensors. Using the proposed control strategy in the experiment, the output of the current estimator appropriately attains the desired value.

VI. Conclusion

In this paper, a sensorless current control technique has been presented. First, the observability of the system with respect to the current has been investigated through mathematical analysis. Next, a current estimator has been proposed for the flyback micro-inverter and validated using computer simulation. Last, the proposed design has been implemented on a solar tile

micro-inverter, verifying the ability to accurately estimate the correct high frequency current.

Using micro-inverters for rooftop solar tiles is the most convenient topology for scalability and design due to parallel outputs. It has been proven that the cost of such micro-inverters can be lowered while still retaining performance using the proposed sensorless current measurement technique.

REFERENCES

[1] G. K. Singh, Solar power generation by PV (photovoltaic) technology: A review, *Energy,* vol. 53, pp. 113, May. 2013.

[2] D. Muoio, Tesla has said little about its solar roof since it began taking orders here's what we do know, Internet: http://www.businessinsider.com/tesla-solar-roof-details-features-pictures-2017-8/, Aug. 4, 2017 [Nov. 21,2017]

[3] A. Mäki and S. Valkealahti, Power losses in log string and parallel-connected short strings of series-connected silicon-based photovoltaic modules due to partial shading conditions, *IEEE Trans. Energy Convers.,* vol. 27, no. 1, pp. 173-183. Mar. 2012.

[4] N. D. Kaushinka and A. K. Rai, An investigation of mismatch losses in solar photovoltaic cell networks, *Energy* vol. 32, no. 5, pp. 755-759. May 2007

[5] R. C. N. Pilawa-Podgurski and D. J. Perreault, Submodule integrated distributed maximum power point tracking for solar photovoltaic applications, *IEEE Trans. Power Electron.* vol. 28, no. 6, pp. 29572967, Jun. 2013.

[6] N. Sukesh, M. Pahlevaninezhad and P. K. Jain, An investigation of mismatch losses in solar photovoltaic cell networks, *IEEE Transactions on Industrial Electronics,* vol. 61, no. 4, pp. 1819-1833, Apr. 2014.

[7] T. Shimizu, K. Wada, and N. Nakamura, Flyback-Type Single-Phase Utility Interactive Inverter With Power Pulsation Decoupling on the DC Input for an AC Photovoltaic Module System, *IEEE Trans Power Electron,* vol. 21, no. 5, pp. 1264 - 1272, Sept. 2006.

[8] T. Shimizu, K. Wada, and N. Nakamura, A flyback-type single phase utility interactive inverter with low-frequency ripple current reduction on the DC input for an AC photovoltaic module system, in *Proc. IEEE PESC, 2002,* pp. 1483-1488.

[9] N. Kasa, T. Iida, and L. Chen, Flyback inverter controlled by sensorless current MPPT for photovoltaic power system, *IEEE Trans. Ind. Electron.,* vol. 52, no. 4, pp. 11451152, Aug. 2005.

[10] M. A. Rezaei, K. J. Lee and A. Q. Huang. A High-Efficiency Flyback Micro-inverter With a New Adaptive Snubber for Photovoltaic Applications, *IEEE Trans. on Power Electron.,* vol. 31, no. 1, pp. 318-327, Jan. 2016.

[11] M. Pahlevani, S. Eren, J. M. Guerrero and P. Jain, A Hybrid Estimator for Active/Reactive Power Control of Single-Phase Distributed Generation Systems With Energy Storage, in *IEEE Transactions on Power Electronics*, vol. 31, no. 4, pp. 2919-2936, April 2016.

[12] S. Eren, M. Pahlevaninezhad, A. Bakhshai and P. K. Jain, Composite Nonlinear Feedback Control and Stability Analysis of a Grid-Connected Voltage Source Inverter With LCL Filter, in *IEEE Transactions on Industrial Electronics*, vol. 60, no. 11, pp. 5059-5074, Nov. 2013.

[13] R. Hermann and A. Krener. Nonlinear controllability and observability, *IEEE Transactions on Automatic Control,* vol. 22, no. 5, pp. 728-740 Oct. 1977

[14] M. Pahlevaninezhad, S. Eren, H. Pahlevani, I. Askarian and S. Bagawade. Digital Current Sensorless Control of Current-Driven Full-Bridge DC/DC Converters, *IEEE Trans. on Power Electron.,* vol. 33, no. 2, pp.1797-1815, Mar. 2017

[15] S. Diop and M. Wang, Equivalence between algebraic observability and local generic observability, *Proc. 32nd IEEE Conf. on Decis. Control, 1993* pp. 2864-2865.

[16] I. Askarian, S. Eren, M. Pahlevani and A. Knight, Digital Real-Time Harmonic Estimator for Power Converters in Future Micro-Grids, *IEEE Transactions on Smart Grid*, June 2017.

[17] M. Pahlevani, S. Pan, S. Eren, A. Bakhshai and P. Jain, An Adaptive Nonlinear Current Observer for Boost PFC AC/DC Converters, in *IEEE Transactions on Industrial Electronics*, vol. 61, no. 12, pp. 6720-6729, Dec. 2014.

[18] S. Eren, M. Pahlevani, A. Bakhshai and P. Jain, A Digital Current Control Technique for Grid-Connected AC/DC Converters Used for Energy Storage Systems, in *IEEE Transactions on Power Electronics*, vol. 32, no. 5, pp. 3970-3988, May 2017.